

# A Novel Use of Hyperspectral Images for Human Brain Cancer Detection using in-Vivo Samples

Himar Fabelo<sup>1</sup>, Samuel Ortega<sup>1</sup>, Raúl Guerra<sup>1</sup>, Gustavo Callicó<sup>1</sup>, Adam Szolna<sup>2</sup>, Juan F. Piñeiro<sup>2</sup>, Miguel Tejedor<sup>1</sup>, Sebastián López<sup>1</sup> and Roberto Sarmiento<sup>1</sup>

<sup>1</sup>*Institute for Applied Microelectronics, University of Las Palmas de Gran Canaria, Las Palmas de Gran Canaria, Spain*

<sup>2</sup>*Department of Neurosurgery, University Hospital Doctor Negrín, Las Palmas de Gran Canaria, Spain*

**Keywords:** Brain Cancer Detection, Hyperspectral Imaging, Random Forest, Classification Algorithms.

**Abstract:** Hyperspectral Imaging is an emerging technology for medical diagnosis issues due to the fact that it is a non-contact, non-ionizing and non-invasive sensing technique. The work presented in this paper tries to establish a novel way in the use of hyperspectral images to help neurosurgeons to accurately determine the tumour boundaries in the process of brain tumour resection, avoiding excessive extraction of healthy tissue and the accidental leaving of un-resected small tumour tissues. So as to do that, a hyperspectral database of in-vivo human brain samples has been created and a procedure to label the pixels diagnosed by the pathologists has been described. A total of 24646 samples from normal and tumour tissues from 13 different patients have been obtained. A pre-processing chain to homogenize the spectral signatures has been developed, obtaining 3 types of datasets (using different pre-processing chain) in order to determine which one provides the best classification results using a Random Forest classifier. The experimental results of this supervised classification algorithm to distinguish between normal and tumour tissues have achieved more than 99% of accuracy.

## 1 INTRODUCTION

Malignant brain tumours, with a global incidence around 3.5 per 100,000 people, are among the most lethal and challenging cancers for treatment. Surgical resection is one of the most important pillars in the treatment of these tumours, but due to their locations, sometimes arising from very eloquent areas of the brain, and their diffuse and infiltrating limits, the total excision is sometimes cumbersome or impossible to achieve.

Modern Neurosurgery for these tumours relies on image-guided resection, but it needs expensive and/or invasive techniques, such as the Neuronavigation, intraoperative Magnetic Resonance Imaging (MRI), injection of reactive for immunofluorescence, etc. The goal of this investigation is to apply an innovative and non-invasive technology tool for image-guided brain tumour resection: Hyperspectral imaging.

This technology is a non-contact, non-ionizing and non-invasive sensing technique very suitable for medicine (Lu et al., 2014); (Akbari et al., 2012). It consists in collecting and processing information

across the electromagnetic spectrum creating a hyperspectral data-cube with the values of the reflectance of the light captured in the scene for different frequencies. This kind of images increases the amount of information acquired in a scene compared with the conventional RGB image or a multispectral image (which has around ten bands), by capturing data in a large number of contiguous and narrow spectral bands over a wide spectral range. Using the information generated by hyperspectral imaging, it is possible to obtain a spectral signature of each pixel. This spectral signature allows differentiating the material or substance that is presented in the pixel. It is expected that tumours will be detected as changes in the spectral signatures compared with normal tissues (Fei et al., 2012); (Martin et al., 2006).

The work presented in this paper has been developed within the HELICoiD (HypErspectralL Imaging Cancer Detection) project. HELICoiD is a European FET (Future Emerging Technologies) project that has the aim of discriminating between normal and tumour tissues in the surface of the human brain during neurosurgical operations in order to

provide the neurosurgeons with a real-time guide that can help in the adequate surgical resection. As a second goal, the project will try to obtain hyperspectral signatures from different tumours, so it might give clues to the neurosurgeon about the tumour histology.

The results of this discrimination process will be shown to the neurosurgeons by using a false colour map where tumour and healthy tissues will be clearly differentiated. This colour map will help them to accurately determine the tumour boundaries in the process of brain tumour resection, avoiding excessive extraction of healthy tissue and the accidental leaving of small tumour tissues.

## 2 MATERIALS AND METHODS

This section provides an overview of the instrumentation and the methodology used to collect the in-vivo hyperspectral data of human brain samples.

### 2.1 Hyperspectral Imaging Instrumentation

In order to obtain the hyperspectral images of the in-vivo human brain surface during the neurosurgical operations, the HELICoiD project has built a demonstrator capable of simultaneously obtaining two hyperspectral cubes. The two hyperspectral cameras selected are the Hyperspec® VNIR A-Series and the Hyperspec® NIR X-Series, manufactured by HeadWall Photonics, Massachusetts, USA. The VNIR (visible and near infrared) camera ranges between 400 nm to 1000 nm. The NIR (near infrared) camera ranges between 900 nm to 1700 nm.

Figure 1 shows the main parts of the demonstrator. The most important elements of the system are located in the acquisition scanning platform. Table 1 presents the specifications of the two push-broom hyperspectral cameras. These cameras are fixed in a scanning unit composed by a stepper motor and a screw with a maximum path of 230 mm and a step resolution of 6.17 µm. Furthermore, a cold light emitter is located together with the cameras. The cold light emitter is connected to a 150 W Quartz Tungsten-Halogen system (QTH) (Figure 2.c), which offers broadband emission in the VIS (visible) and NIR spectral ranges (400 nm to 2200 nm), through an optical fibre. This system isolates the high temperatures produced by the halogen lamp, avoiding a direct emission to the brain surface.

Data pre-processing system is composed by a high performance computer which manages the entire system, especially the acquisition scanning platform and the interaction with the user through the graphical user interface (GUI).

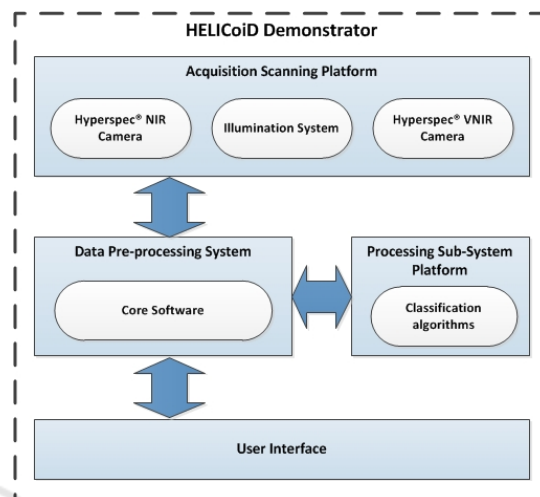


Figure 1: HELICoiD demonstrator main parts.

Finally, the processing sub-system platform has the goal of performing the hyperspectral classification in order to achieve the results in real-time. The platform selected for this issue is the Kalray many-core processor that features MIMD (Multiple Instruction Multiple Data) architecture (B. D. de Dinechin et al., 2013). This platform is focused on intensive computing, low power and embedded applications.

Table 1: Camera Specifications.

	Hyperspec® VNIR	Hyperspec® NIR
Spectral range (nm)	400 – 1000	900 – 1700
Spectral resolution (nm)	2 – 3	5
Slit (µm)	25	25
Spatial bands	1004	320
Spectral bands	826	172
Frame Height (FOV) (mm)	129.21	153.6
Pixel Dimensions (IFOV) (mm)	0.1287	0.4800
Max Pixels per Frame	1004	320
Max Frames per Capture	1825	489
Dispersion per pixel (nm)	0.74	4.8
Detector array	Silicon CCD	InGaAs
Frame rate (fps)	90	100

Figure 2.b shows the HELICoiD demonstrator inside the pre-operative area at the University Hospital Doctor Negrín in Las Palmas de Gran Canaria, Spain. Figure 2.a presents the acquisition platform where the cameras and the cold light element are located. On the left side of the platform, the VNIR camera is located, and on the right side the NIR camera is placed. In the middle of the two cameras, the cold light emitter is located. These three elements are correctly aligned in order to obtain the images properly illuminated. Figure 2.d displays the stepper motor controller, which is in charge of managing the scanning platform shift.

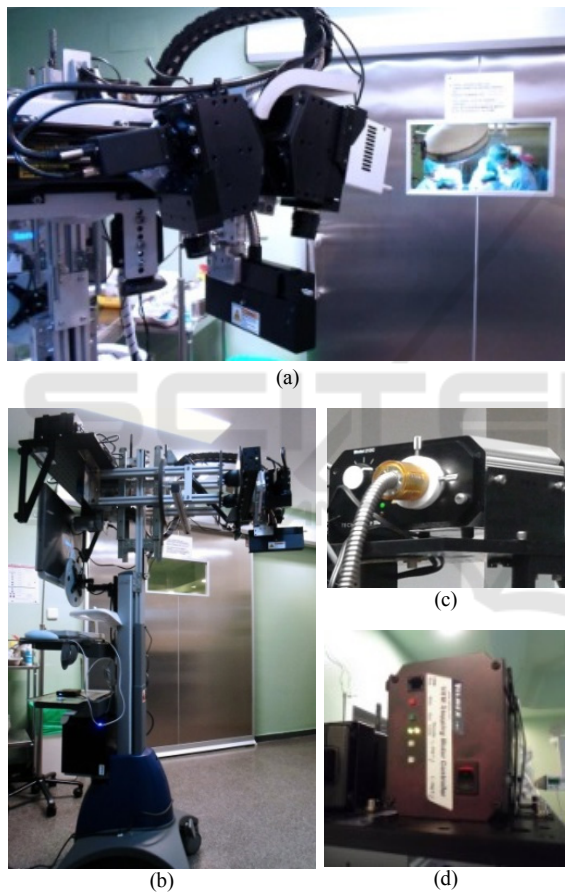


Figure 2: (a) Acquisition scanning platform, (b) complete HELICoiD demonstrator, (c) Quartz Tungsten-Halogen system and (d) stepper motor controller.

## 2.2 Hyperspectral Image Dataset

Using the HELICoiD demonstrator, an in-vivo human brain hyperspectral image database has been created. The hyperspectral cubes have been obtained from 13 different patients at the University Hospital Doctor Negrín. The disease of the tissues captured

during this study involves both primary brain tumours and secondary tumours (metastasis). All primary tumours captured have been diagnosed as grade IV glioblastoma. For secondary tumours two different types of metastasis, lung and renal, have been collected.

From this database, a dataset formed by normal brain tissue and tumour tissue (primary and secondary) of hyperspectral samples have been collected and labelled. The work presented in this paper is only focused in the VNIR hyperspectral cubes as they have provided better results. Table 2 shows the number of the labelled in-vivo human brain samples available from the VNIR hyperspectral cubes.

Table 2: HELICoiD Labelled Spectral Signature Data Base.

Tissue Type		Patients	# Samples
Normal		9	12604
Tumour	Primary	8	10059
	Secondary	4	1983

In order to obtain the samples correctly labelled, the four steps flowchart presented in Figure 3 has been followed. First, when the neurosurgeons have the brain surface exposed, they place two sterilised rubber ring markers over it. One marker is placed over the zone where clearly the tumour lesion is located. The other marker is placed over an area far from the tumour lesion, where the neurosurgeon can be quite confident that the brain tissue is healthy. After that, the operator of the HELICoiD demonstrator captures the hyperspectral image of this exposed brain surface.

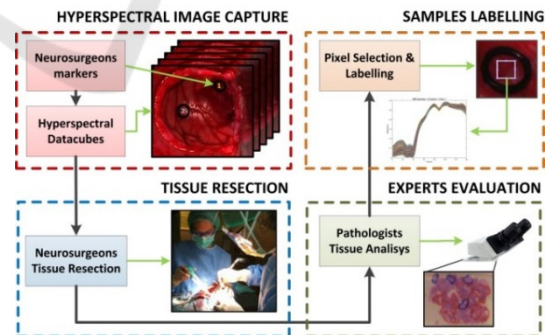


Figure 3: Data capture and labelling process.

So as to identify the location of the markers over the brain, the neuronavigator pointer is used. Figure 4 illustrates the use of the neuronavigator to identify the position of the markers in a MRI.

Next, neurosurgeons remove the tissue inside the tumour marker. This tissue is sent to the pathologists, which are the experts who can determine the real

diagnosis of the tissue inside the marker. If the brain tissue is tumour, pathologists specify the grade and the type of the tumour.

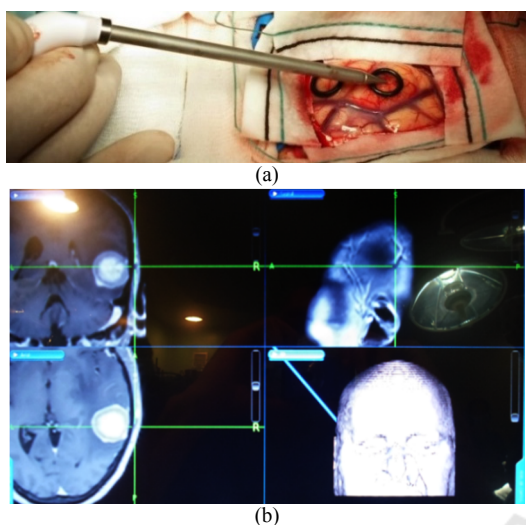


Figure 4: (a) Neuronavigator pointer over the tumour marker located on the brain surface exposed and (b), neuronavigator screen capture with the coordinates of the tumour marker in a MRI.

Finally, with this information, the pixels inside the markers are cropped manually, avoiding pixels which could have specular reflections produced by the non-uniformity of the brain surface. These selected pixels are labelled and stored with the information provided by the pathologists. Labelled pixels will be used as inputs in a supervised classification algorithm scheme.

Figure 5 presents the most representative bands of the VNIR hyperspectral image of the patient 12's brain surface captured by the demonstrator.

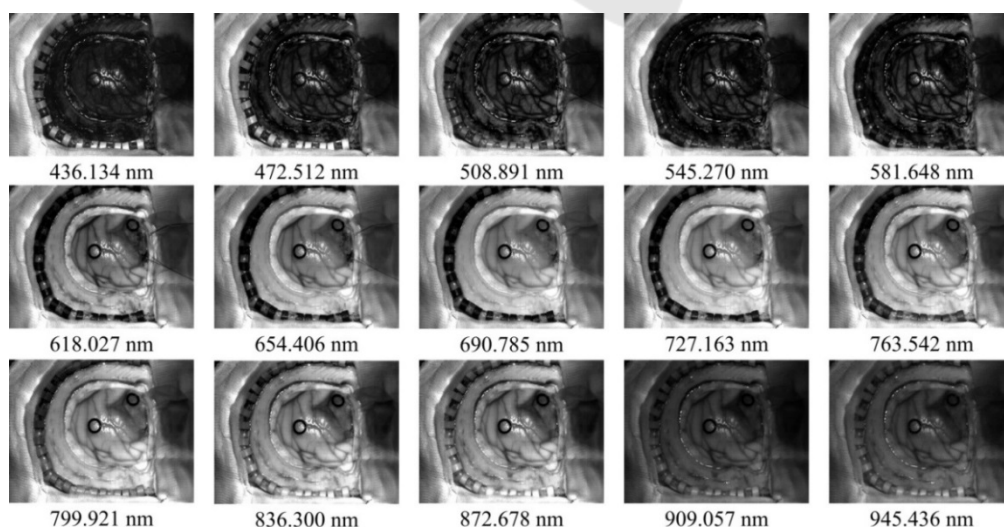


Figure 5: Most representative bands of the VNIR hyperspectral image (400 nm to 1000 nm) from patient 12.

### 3 CLASSIFICATION SYSTEM

For performing a spectral classification using the hyperspectral images captured, a classification system based on a Random Forest (RF) classifier has been defined. Figure 6 shows an overview of this classification system.

The first stage of the proposed classification system is the acquisition step, where the labelled dataset of the tumour and normal samples are collected. The procedure followed to collect these data has been previously described in section 2.2.

After the acquisition stage, a pre-processing chain is applied to the labelled dataset. In this pre-processing stage an image calibration is done in order to address the problem of the spectral non-uniformity of the illumination device and the dark current. Furthermore, a set of steps with the goal of removing the noise of the spectral signatures and to reduce the number of bands of the samples without lose the main spectral information are applied.

Finally, so as to homogenize the spectral signatures in terms of reflectance level, a pixel bright correction step and a normalization step are performed.

In the classification stage, the labelled dataset is partitioned into two different datasets. Training dataset is used to generate the classifier model while test dataset is used to validate this model, obtaining the results of the classification. Sensitivity, specificity and overall accuracy are the evaluation metrics chosen in order to know the goodness of the classifier model. These evaluation metrics will be described later.

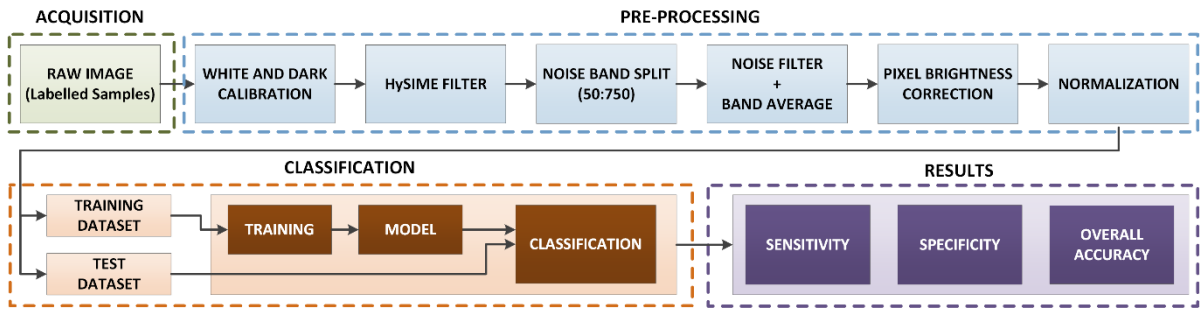


Figure 6: Classification system overview.

### 3.1 Data Pre-processing

A pre-processing chain composed by three main steps (image calibration, spectral noise and band reduction and data normalization) has been developed in order to homogenize the spectral signatures of the labelled samples obtained from the in-vivo hyperspectral data-cubes.

#### 3.1.1 Image Calibration

The first step in the pre-processing chain is the image calibration, where the significant signal variations caused by the non-uniform illumination over the surface of the captured scene are corrected. The acquired raw image is calibrated using the white and dark reference images.

White and dark reference images are acquired by the demonstrator inside the operating theatre under the same illumination conditions used to acquire the in-vivo brain surface images. The white reference image is obtained from a standard white reference tile and the dark reference image is obtained by keeping the camera shutter closed. The hyperspectral calibrated image is calculated using the equation (1), where  $CI$  is the calibrated image,  $RI$  is the raw image and  $WR$  and  $DR$  are the white and dark reference images respectively. Figure 7 shows the spectral signature of a grade IV glioblastoma tumour tissue before the calibration step (raw pixel) and Figure 8 after the applied calibration.

$$CI = 100 \cdot \frac{RI - DR}{WR - DR} \quad (1)$$

#### 3.1.2 Noise and Dimensionality Reduction

The second step in the pre-processing chain is to apply a series of filters in order to remove the noise existing in the spectral signatures, mainly due to the CCD sensor of the VNIR camera.

First of all, the noise filter which conforms the first step of the HySIME algorithm is applied,

reducing a large amount of noise from the spectral signatures. This function, which is named Hyperspectral Noise Estimation, infers the noise in a hyperspectral data set, by assuming that the reflectance at a given band is well modelled by a linear regression on the remaining bands (Bioucas-Dias and Nascimento, 2008); (Nascimento and Bioucas-Dias, 2015). Figure 9 shows the same spectral signature after having applied this noise filter.

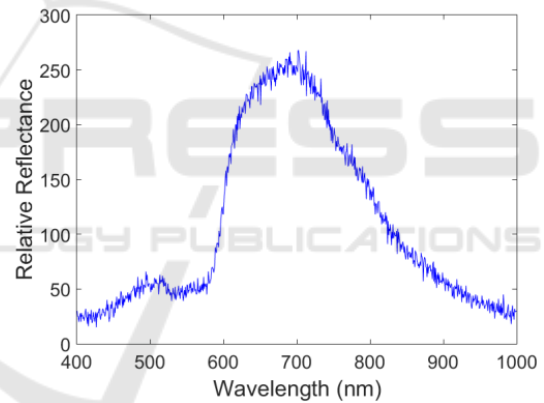


Figure 7: Raw spectral signature of a grade IV glioblastoma tumour tissue.

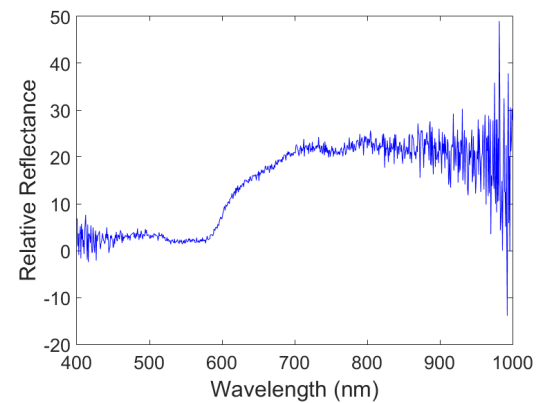


Figure 8: Calibrated spectral signature of a grade IV glioblastoma tumour tissue.

After this step, the bands from 0 to 50 and the bands from 750 to 826 are removed since these bands contain too much noise due to the limited performance of the CCD sensor, the grate and the light scattering in the extreme bands. This fact can be seen in Figure 9. Additionally, this step reduces the number of bands in the spectral signatures from 826 to 700 bands.

Afterwards, a smoothing technique is independently applied to each pixel of the image. This technique modified each pixel  $y_k$  of the spectral signature of the pixel under analysis,  $Y = (y_1, y_2, \dots, y_{N_B})$ , where  $k$  is the selected pixel and  $N_B$  is the original number of bands. The new value of the "smoothed point"  $(y_k)_s$  is the average of the values corresponding to predefined number of its surrounding points, as shown in equation (2), where  $n$  is number of bands to be combined.

$$(y_k)_s = \sum_{i=-n}^{i=n} y_{k+i} / (2 \cdot n + 1) \quad (2)$$

Due to the extremely high spectral resolution of the images, it has been observed that consecutive bands are correlated, providing redundant information. In order to avoid this redundancy and speed up the hyperspectral analysis of the data set, a few bands have been removed. Moreover, it is not needed to perform the smooth filter for those bands that are going to be removed, which eases the filtering process in terms of computational burden. In particular 129 spectral bands, from the 700 spectral bands previously processed, have been totally filtered, uniformly covering the spectral range from 400 to 1000 nm as shown in Figure 10.

### 3.1.3 Data Normalization

Due to the surgery procedure, the pixels are captured at different height, and hence, at different radiation intensity. This fact typically causes that pixels labelled as tumour and normal tissue have very different radiation intensities. If these pixels are introduced without any pre-processing in a classifier, the pixels could be classified according to its brightness, without really taking into account their spectral signatures. In order to avoid this fact, a pre-processing step which normalizes the brightness of the pixels in the image needs to be included. This process calculates the brightness of each pixel of the hyperspectral image and divides each pixel by its brightness, as shown in equation (3). In this equation  $Y_{BC}$  is the pixel with the brightness correction,  $Y$  is the pixel to be corrected and  $y_i$  is the  $i$ -th component of this pixel. With this pre-processing step, the brightness of each pixel is homogenized without

modifying its spectral signature. Figure 10 illustrates the final spectral signature with the full pre-processing chain applied.

$$Y_{BC} = \frac{Y}{\sqrt{\sum_{i=1}^{129} y_i^2}} \quad (3)$$

Figure 11 presents the VNIR RGB image of the patient 12, with the tumour area remarked (surgeon prior evaluation), and the most representative features of the final pre-processed data-cube. As it can be appreciated, in feature 45 veins and tumour tissue have a low brightness regarding to the normal tissue. However, in feature 55 and 65, veins and normal tissues have approximately the same brightness level while the area where tumour is located exhibit lower brightness. Feature 80 allows seeing veins in high brightness conditions while tumour and normal tissues have the same brightness. Finally, the feature 125 is relevant because where the tumour area is located there is a high level of brightness. This fact suggests that this pre-processed chain additionally can obtain high level of contrast to distinguish between veins, normal tissues and tumour tissues.

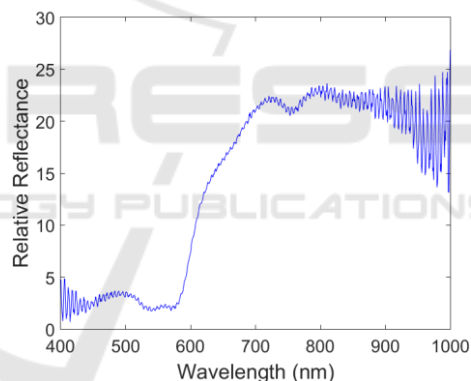


Figure 9: Spectral signature with the HySIME filter applied to a grade IV glioblastoma tumour tissue.

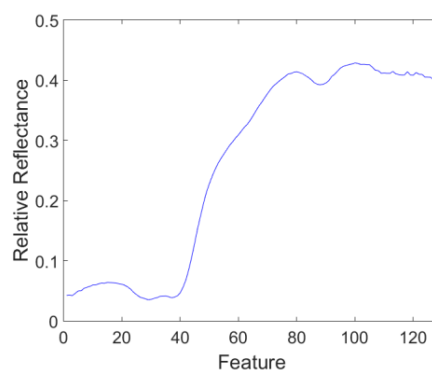


Figure 10: Spectral signature with the noise and band reduction step and the normalization applied to a grade IV glioblastoma tumour tissue.

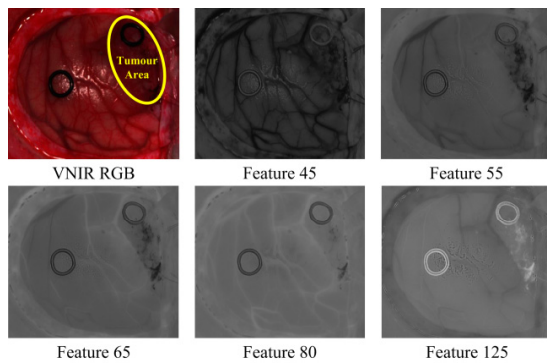


Figure 11: Most representative features of the final pre-processed image from patient 12.

### 3.2 Classification Algorithm

In this research work a supervised learning algorithm has been employed, where the input features of the classifier consist in the spectral signatures extracted from brain tissue. The data mining algorithm chosen for classifying data is Random Forest (RF). This algorithm has been already used in the classification of hyperspectral data (Ham et al., 2005). Random Forest is an ensemble of Decision Trees (DTs), where each tree has been generated with the same training set, but is growing using different random vectors (Breiman, 2001). A single Decision Tree handles high-dimensional data well, has the ability to ignore irrelevant features and provides an easy model interpretation. However, DT usually has relatively low prediction accuracy. Due to the advantages provided by DT, many efforts to improve its prediction accuracy has been proposed. It has been discovered that one of the best ways to improve the performance of Decision Tree-based algorithms is using ensembles of DT, like Random Forest classifier (Svetnik et al., 2003). The output of RF classifier is calculated as the most popular class voted by the trees.

Advantages of RF compared to other statistical classifiers include very high classification accuracy; a novel method of determining variable importance; ability to model complex interactions among predictor variables; flexibility to perform several types of statistical data analysis, including regression, classification, survival analysis, and unsupervised learning; and an algorithm for imputing missing values (Cutler et al., 2007).

### 3.3 Experimental Setup

The experimental setup chosen for this study merges all available hyperspectral labelled data (from 13 different patients) in a single dataset. The dataset

employed in this research work has been created by joining each single operation hyperspectral labelled data, even if a unique class is given for a certain operation. As the training and testing stages for classification have been performed using data from all the operations, the inter-patient variability of the data will be taken into account.

The labelling of data has been performed using two different abstraction levels of the diagnosis of the tissue. In the first level, tissues have been grouped in 'Normal' tissues and 'Tumour' tissues, and the classification using this labelling scheme has been named 'Tag Level 1'. For the second labelling scheme, 'Tumour' tissues have been divided in 'Primary' and 'Secondary' tissues, attending to the diagnosis provided by pathologists. This labelling scheme has been named 'Tag Level 2'. The summary of the dataset is given in Table 3.

In order to estimate the classifier performance, and for obtaining the optimal configuration of the selected algorithm, a three-way cross validation has been employed. Three-way cross-validation consists in two different stages for splitting the available dataset: in the first stage, k-fold cross-validation is used in order to get training and testing subsets. Test data will be used to estimate the classifier performance, and the training data are partitioned again into training data and validation data (Figure 12). The training subset of the second cross-validation stage is used to create the model of the classifier, and the validation data are used to evaluate the performance of the classifier. With the second stage partition, the model fitting will be accomplished, and the parameters of the classifier will be modified in order to obtain the optimal configuration of the algorithm. The test set obtained in the first dataset split, is used to perform the performance evaluation of the algorithm by using unknown data for the classifier. The k value selected for both cross-validations is 10, which is a typical value used in data mining

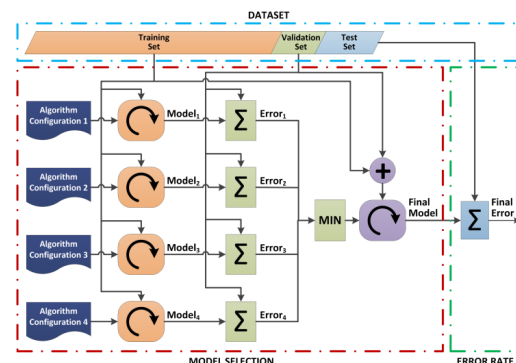


Figure 12: Three-way cross-validation experimental setup overview.

Table 3: HELICoiD Labelled Dataset with two classification tag levels.

#Operation	Diagnosis		#Samples
	Tag Level 1	Tag Level 2	
1	Normal		408
	Tumour	Secondary	578
4	Normal		1939
	Tumour	Secondary	522
5	Normal		832
	Tumour	Secondary	493
6	Normal		806
7	Normal		768
8	Normal		1484
	Tumour	Primary	3259
10	Tumour	Primary	425
12	Normal		806
	Tumour	Primary	1424
13	Tumour	Secondary	390
14	Tumour	Primary	1139
15	Normal		648
	Tumour	Primary	800
16	Normal		4913
	Tumour	Primary	1987
17	Tumour	Primary	1025
<b>Total</b>			<b>24646</b>

### 3.4 Evaluation Metrics

The goodness of the classifier has been measured using sensitivity, specificity and overall accuracy metrics. Sensitivity measures the test ability to identify a condition correctly. It is computed as follows:

$$\text{Sensitivity} = \frac{TP}{TP + FN} \quad (5)$$

where TP is the number of true positives and FN is the number of false negatives in a population.

Specificity measures the test ability to exclude a condition correctly. It is expressed as follows:

$$\text{Specificity} = \frac{TN}{TN + FP} \quad (6)$$

where TN is the number of true negatives and FP is the number of false positives in a population.

Finally, the equation (7) shows the accuracy metric that represents the percentage of total correctly classified samples in a population:

$$\text{Accuracy} = \frac{TP + TN}{TP + FP + TN + FN} \quad (7)$$

## 4 EXPERIMENTAL RESULTS

The hyperspectral classification experiments have been performed using the three different pre-processed data previously described. The calibrated data are the labelled samples with only the white and dark calibration applied. HySIME filtered data are the previous calibrated samples with the HySIME filter applied over them. The last set of data has the complete pre-processed chain applied, this set of data is called pre-processed samples.

As it was commented previously, two different levels of diagnosis detail have been evaluated.

### 4.1 Tumour Vs Normal: Tag Level 1

In this section will be presented the results obtained using the Random Forest classification system over the three different set of data taking into account the first tag level (normal vs tumour tissues).

The results of the classification in this case study shows that an automatic discrimination between 'Normal' tissue and 'Tumour' tissue is possible using the hyperspectral signature of the tissues. Sensitivity and specificity lie in the same range, which means that the algorithm is capable to identify both kinds of tissues.

Although the classification results provide accurate discrimination rates in terms of accuracy, specificity and sensitivity, varying the pre-processing stage results in an improvement of the classification. From data shown on Table 4, it can be seen that the accuracy improves from around 93%, when the pre-processing chain consists only of the calibration of the hyperspectral image, to 99% when using the whole pre-processing chain presented in Figure 6. Figure 13 presents these results in a bar chart.

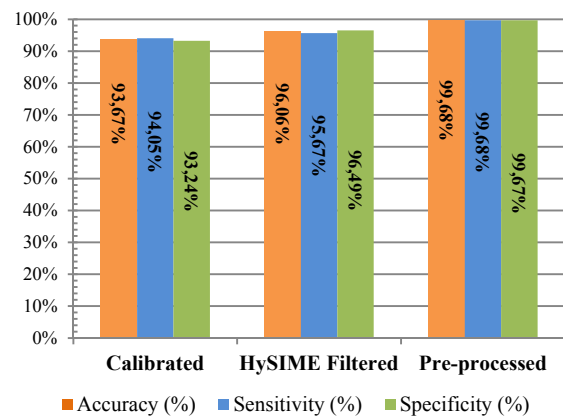


Figure 13: Comparison between the classification results of the three data sets at tag-detail level 1.

Table 4: Comparison between the classification results of the three data sets at the tag level 1.

	Calibrated	HySIME Filtered	Pre-processed
Sensitivity (%)	94.05	95.67	99.68
Specificity (%)	93.24	96.49	99.67
Accuracy (%)	93.67	96.06	99.68

This trend is kept for the rest of the evaluation metrics: specificity improves from 93% to 99% and sensitivity improves from 94% to 99%, when the full pre-processing chain is used, instead of performing only the calibration.

### 4.2 Normal Vs Primary Vs Secondary: Tag Level 2

The same data have been classified with a different tag scheme, where 'Tumour' tissues have been divided into 'Primary' and 'Secondary' tumour tissue labels. Figure 14 illustrates the accuracy results between the different pre-processed datasets and Table 5 to Table 7 show the classification results in terms of sensitivity and specificity for each class. These data have been obtained by calculating the confusion matrix of each dataset that can be seen in Table 8. The error estimation of this classification shows that the algorithm can keep a good performance on discriminating between normal and tumour tissue, even using a more complex labelling scheme. The sensitivity and specificity values show also high values, which indicates that all classes have been properly classified. Results show again that the used pre-process chain improves the results of the classification.

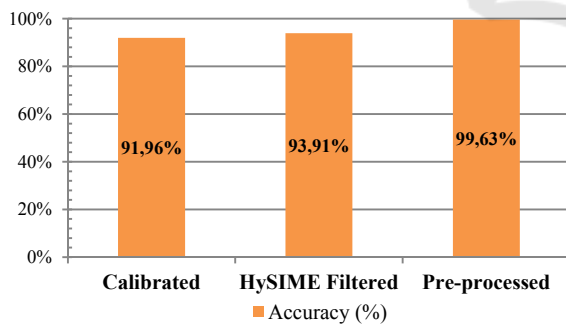


Figure 14: Accuracy comparison between the classification results of the three data sets in tag level 2.

Table 5: Classification results of the calibrated dataset in tag level 2.

		Sensitivity (%)		
		Normal	Primary	Secondary
Specificity (%)	Normal	-	94.67	99.67
	Primary	94.63	-	94.34
	Secondary	97.64	89.21	-

Table 6: Classification results of the HySIME filtered dataset in tag level 2.

		Sensitivity (%)		
		Normal	Primary	Secondary
Specificity (%)	Normal	-	96.07	99.51
	Primary	95.49	-	96.4
	Secondary	99.45	91.88	-

Table 7: Classification results of the pre-processed dataset in tag level 2.

		Sensitivity (%)		
		Normal	Primary	Secondary
Specificity (%)	Normal	-	99.92	100.00
	Primary	99.31	-	99.90
	Secondary	100.00	100.00	-

## 5 CONCLUSIONS

In this paper, it has been described a hyperspectral acquisition system used to create a hyperspectral database of human brain tissues previously diagnosed as tumour or normal. In each surgical procedure, a few rubber ring markers have been placed by the neurosurgeons to get assessed diagnosis from pathology. Some of these markers were located in areas of brain where neurosurgeons were quite sure that the tissues were healthy, and the other markers were placed where the resection was going to be performed. A biopsy from the rejected tissue was sent to pathology, providing assessed diagnosis of the tissues inside the marker. These samples were used as the ground truth for classification.

Table 8: Confusion matrix of the three types of datasets in tag level 2.

		Predicted Results								
		Calibrated			HySIME Filtered			Per-Processed		
		Normal	Primary	Secondary	Normal	Primary	Secondary	Normal	Primary	Secondary
Gold Standard	Normal	1225	52	3	1223	43	1	1249	7	0
	Primary	69	917	15	50	910	16	1	1013	0
	Secondary	4	55	124	6	34	181	0	1	193

Taking into account the diagnostic information provided by pathologists, the pixels inside markers were extracted from the hypercubes and labelled according to the diagnosis. Due to the complexity of the diagnostic information, a labelling scheme consisting in two abstraction levels of disease details had been proposed.

The classification results shown in section 4 show that it is possible to obtain an accurate and automatic discrimination between different types of tissues using the labelling schemes proposed. Although the three proposed pre-processing chains provided accurate classification results (accuracy higher than 89% for all the classifications), the more complex one provided the best classification results in all the experiments exposed in this paper.

In the near future, some additional research is foreseeable to be done. Firstly, the complexity of the diagnosis can be further explored. For instance, primary tumours could be classified according to its Grade, and Secondary tumours (metastasis) could be differentiated attending to their origin (breast, lung, etc.). The next step will be to define a more complex labelling scheme to better classify the type of tumour. Secondly, we are working in the design a case study where the automatic diagnostic of a new patient could be computed by using a model that had been created using the hyperspectral data from previous (and in consequence different) patients. Thirdly, it could be interesting to test the performance of other different machine learning algorithms, like the support vector machines (SVM), the neural networks (NN), etc. Finally, due to the large experience that the research group has in hardware implementations, we are considering the implementation of the pre-processing and classification algorithms in some hardware platform (FPGA, GPU, ASICs, many cores, etc.) to accelerate its execution.

## ACKNOWLEDGEMENTS

This work has been supported in part by the European Commission through the FP7 FET Open programme ICT-2011.9.2, European Project HELICoiD “HypErspectral Imaging Cancer Detection” under Grant Agreement 618080.

## REFERENCES

- G. Lu, B. Fei, 2014. Medical hyperspectral imaging: a review. *Journal of biomedical optics*, vol. 19, no. 1, pp. 010 901–010 901.
- H. Akbari, L. V. Halig, D. M. Schuster, A. Osunkoya, V. Master, P. T. Nieh, G. Z. Chen, and B. Fei, 2012. Hyperspectral imaging and quantitative analysis for prostate cancer detection. *Journal of biomedical optics*, vol. 17, no. 7, pp. 0 760 051–07 600 510.
- B. Fei, H. Akbari, L. V. Halig, 2012. Hyperspectral imaging and spectral-spatial classification for cancer detection. *Biomedical Engineering and Informatics (BMEI), 5th International Conference on. IEEE*, pp. 62–64.
- M. E. Martin, M. B. Wabuye, K. Chen, P. Kasili, M. Panjehpour, M. Phan, B. Overholt, G. Cunningham, D. Wilson, R. C. DeNovo, & T. Vo-Dinh, 2006. Development of an advanced hyperspectral imaging (HSI) system with applications for cancer detection. *Annals of Biomedical Engineering*, 34(6), pp. 1061–1068.
- B. D. de Dinechin, R. Aygnac, P.-E. Beaucamps, P. Couvert, B. Ganne, P. G. de Massas, F. Jacquet, S. Jones, N. M. Chaisemartin, F. Riss, T. Strudel, 2013. A clustered manycore processor architecture for embedded and accelerated applications. *High Performance Extreme Computing Conference (HPEC), IEEE*, pp.1-6.
- J. M. Bioucas-Dias and J. M. Nascimento, 2008. Hyperspectral subspace identification. *Geoscience and Remote Sensing, IEEE Transactions on*, vol. 46, no. 8, pp. 2435–2445.
- J. M. Nascimento and J. M. Bioucas-Dias, 2015. Hyperspectral noise estimation. [https://github.com/jhausser/ParTI/blob/master/mvsa\\_demo/estNoise.m](https://github.com/jhausser/ParTI/blob/master/mvsa_demo/estNoise.m), last accessed: November 2015.
- JiSoo Ham, Yangchi Chen, Melba M. Crawford, 2005. Investigation of the Random Forest Framework for Classification of Hyperspectral Data. *IEEE Transactions On Geoscience and Remote Sensing*, Vol. 43, No. 3, pp. 492 – 501.
- Breiman, L., 2001. Random forests. *Machine learning*, Vol. 45, No 1, pp. 5-32.
- Svetnik, V., Liaw, A., Tong, C., Culberson, J. C., Sheridan, R. P., & Feuston, B. P., 2003. Random forest: a classification and regression tool for compound classification and QSAR modeling. *Journal of chemical information and computer sciences*, Vol. 43, No 6, pp. 1947-1958.
- R. Cutler, T. C. Edwards, K. H. Beard, A. Cutler, K. T. Hess, J. Gibson and J. J. Lawler, 2007. Random Forests for Classification in Ecology. *Ecology, Ecological Society of America*, Vol. 88, No. 11, pp. 2783-2792.